Applied Thermal Engineering 159 (2019) 113896

Contents lists available at ScienceDirect

Applied Thermal Engineering

journal homepage: www.elsevier.com/locate/apthermeng

Research Paper

Numerical study on flow and heat transfer of a hybrid microchannel cooling scheme using manifold arrangement and secondary channels

Min Yang, Bing-Yang Cao*

Key Laboratory for Thermal Science and Power Engineering of Ministry of Education, Department of Engineering Mechanics, Tsinghua University, Beijing 100084, PR China

HIGHLIGHTS

- A hybrid design using manifold arrangement and secondary channels for microchannel heat sink is proposed.
- A Design Optimization Area (DOA) for the MMC-SOC is defined.
- The pressure drop and thermal resistance can be both reduced in DOA.
- The best hybrid design with geometrical parameters of ($\lambda = 1$, $\beta = 1$) is obtained.

ARTICLE INFO

Keywords:
Microchannel heat sink
Hybrid design
Manifold arrangement
Secondary channels
Design Optimization Area (DOA)
Hydraulic and thermal performance enhancements

ABSTRACT

The flow and heat transfer characteristics of a novel hybrid microchannel heat sink with manifold arrangement and secondary oblique channels (MMC-SOC) are numerically studied. Through the relationship between the total thermal resistance ratio (R_t/R_{t0}) and pressure drop ratio ($\Delta P/\Delta P_0$), we define a region named Design Optimization Area (DOA), where the pressure drop ΔP and the total thermal resistance R_t can be both reduced due to the secondary channels. The numerical results show that the best heat sink can reduce ΔP by 1.91%, and simultaneously decrease R_t by 19.15% compared to the original MMC heat sink at $Re = 295$. In addition, the effects of secondary channel on ΔP are dependent on both the geometrical parameters and Reynolds numbers. On the one hand, it can reduce the pressure loss at small Reynolds numbers for most heat sinks. However, it can also increase the pressure loss at high Reynolds numbers for most heat sinks. As Re increases, the ratio (R_t/R_{t0}) becomes smaller and ($\Delta P/\Delta P_0$) becomes larger, indicating a better thermal performance and a worse hydraulic performance. The secondary flow field analyses visually show the hydraulic and thermal performance enhancements due to thermal boundary layer re-development and flow mixing.

1. Introduction

Due to the rapid development of integrated circuit (IC) manufacturing and packaging technologies [1–3], both the processing performance and die packaging density keep increasing, which results in high heat fluxes and continuously growing heat dissipation. If the high heat generation cannot be effectively removed, the reliability, performance and lifetime of electronic devices will be adversely affected [4,5]. Consequently, thermal management becomes an essential element in the developing of various electronic components. Traditionally, since the heat removal capacity of air cooled heat sink is limited due to the low thermal conductivity of air [6,7], liquid cooling (microchannel [8–10] or even nanochannel [11–13] heat sinks) is being applied to high heat flux electronic systems. In 1981, the concept of microchannel heat sink was proposed by Tuckerman and Pease [14] for the first time. They experimentally proved that the proposed microchannel heat sink could remove a heat flux of 790 W/cm^2 with a maximum temperature difference of 71 °C. However, the required pressure drop was 214 kPa due to the combination of narrow channel width and high flow rate. Due to the entrance region effects and high surface-to-volume ratio, the microchannel heat sink has high heat flux removal capability and has become one of the most promising technologies for the thermal management of electronics [15]. However, the pressure drop required for high heat dissipation is too high for practical applications. In order to increase the heat sink thermal performance and decrease the required pressure drop, many studies on the structure optimization of microchannel heat sink have been conducted, such as the inlet/outlet arrangement effects [16,17], wavy microchannels [18,19], effects of pins

* Corresponding author.
E-mail address: caoby@tsinghua.edu.cn (B.-Y. Cao).

https://doi.org/10.1016/j.applthermaleng.2019.113896
Received 13 December 2018; Received in revised form 6 May 2019; Accepted 1 June 2019
Available online 04 June 2019
1359-4311/

Nomenclature

A_{con}	convective heat transfer area (m^2)
A_{hs}	heat source area (m^2)
C_p	specific heat capacity (J/(kg K))
d	secondary channel width (m)
D_h	hydraulic diameter (m)
f	Darcy friction factor
h	convection coefficient (W/m^2 K)
h_c	channel height (m)
h_b	base height (m)
$h_{i\text{-}o}$	inlet/outlet height (m)
k	thermal conductivity (W/m K)
L_c	total channel length (m)
L_t	total flow length (m)
Nu	Nusselt number
P_p	pumping power (W)
ΔP	pressure drop (Pa)
q''	heat flux (W/m^2)
Q	total heat flux (W)
R	thermal resistance (K/W)
Re	Reynolds number
T	Temperature (K)
u_m	mean velocity (m/s)
$\dot{V}$	volume flow rate (m^3/s)
W_c	channel width (m)
W_w	channel wall width (m)
W_{in}	manifold inlet width (m)
W_{out}	manifold outlet width (m)

Subscripts

0	original state
ave	average
c	channel
f	fluid
s	solid
t	total
in	inlet
out	outlet
w	wall

Greek symbols

λ	relative secondary channel width
β	relative longer-edge length
ρ	density (kg/m^3)
μ	dynamic viscosity (kg/(m s))

fins or cavities in sidewall [20–23], double-layer microchannel heat exchanger [24,25], manifold arrangement [26–33], secondary flow [34–37]. Among these heat transfer enhancement techniques, microchannel heat sink with manifold arrangement and secondary flow are two of the most promising cooling techniques which have recently attracted significant attention.

Unlike traditional microchannel (TMC) heat sink, the coolant flows through the alternating inlet and outlet manifolds in the direction normal to the manifold microchannel (MMC) heat sink base, which can greatly reduce the effective flow length and pressure drop in microchannels. The earliest research on MMC was carried out by Harpole and Eninger in 1991 [26]. They developed a two-dimensional flow/thermal model for single coolant flow to optimize the design parameters of MMC heat sink. The working fluid could be pure water or water-methanol mixture. The model predicted that the effective heat transfer coefficients on the order of 100 W/cm^2K were achievable with pressure drop of only 1 or 2 bar by using high-aspect-ratio microchannels (30 channels/cm). Since then, the optimized geometries and operating conditions of MMC heat sink have been widely studied for electronics cooling applications. Copeland et al. [27] performed numerical analyses on silicon MMC heat sink and found that the inlet region had better heat transfer performance. Ryu et al. [28] carried out three-dimensional numerical analyses of a MMC heat sink using a SIMPLE-type finite volume method incorporating an optimization scheme. The optimized design can reduce the thermal resistance by more than 50% while maintaining better temperature uniformity of the heated surface. Kermani et al. [29] fabricated the manifold and microchannel by etching two separate silicon substrates, and then bonded them together to form a sealed MMC heat sink. Their experimental results show that a heat transfer coefficient nearly 66000 W/m^2K can be achieved at a water flow rate of 1.1 g/s. Sarangi et al. [30] developed a three-dimensional numerical model to study and optimize the geometric parameters of the MMC heat sink. Their deterministic analyses showed that the best thermal performance of MMC heat sink could be obtained when the ratio of manifold inlet to outlet length is 3. Arie et al. [31] developed a hybrid method that could reduce computational time relative to the CFD model when calculating the heat transfer performance of MMC heat sink. They performed an approximation-based multi-objective optimization based on the hybrid method and found that MMC heat sink showed better thermal and flow performance over chevron plate heat exchangers. Li et al. [32] studied the flow and thermal performance of non-Newtonian fluid flow in MMC heat sink by using three-dimensional numerical simulations. They found that the pseudo-plastic fluid could reduce the drag resistance and improve the heat transfer

Table 1
Summary of selected manifold-microchannel (MMC) literature review.

Authors	Methods	Conclusions
Harpole and Eninger (1991) [26]	Simulation	A two-dimensional flow/thermal model was developed and the effective heat transfer coefficients on the order of 100 W/cm^2K with pressure drop of only 1 or 2 bar were predicted.
Copeland et al. (1997) [27]	Simulation	The isothermal model could predict the thermal and flow performance well and the inlet region had better heat transfer performance.
Ryu et al. (2003) [28]	Simulation	50% thermal resistance reduction and better temperature uniformity could be obtained compared with traditional microchannel heat sink.
Kermani et al. (2009) [29]	Experiment	Heat transfer coefficient of 65480 W/m^2K was obtained at a water flow rate of 1.1 g/s and heat flux of 75 W/cm^2.
Sarangi et al. (2014) [30]	Simulation	The best thermal performance of MMC heat sink could be obtained when the ratio of manifold inlet to outlet length is 3.
Arie et al. (2015) [31]	Simulation	A hybrid computational method that could greatly reduce computational time was developed and verified by direct CFD simulation and experimental results.
Li et al. (2017) [32]	Simulation	2 orders of magnitude reduction on drag resistance and significant thermal enhancement of pseudo-plastic fluid flow were obtained compared with Newtonian fluid.
Drummond et al. (2018) [33]	Experiment	Heat flux dissipation of 910 W/cm^2 with pressure drops of less than 162 kPa and chip temperature rose under 47 °C above inlet temperature was observed.

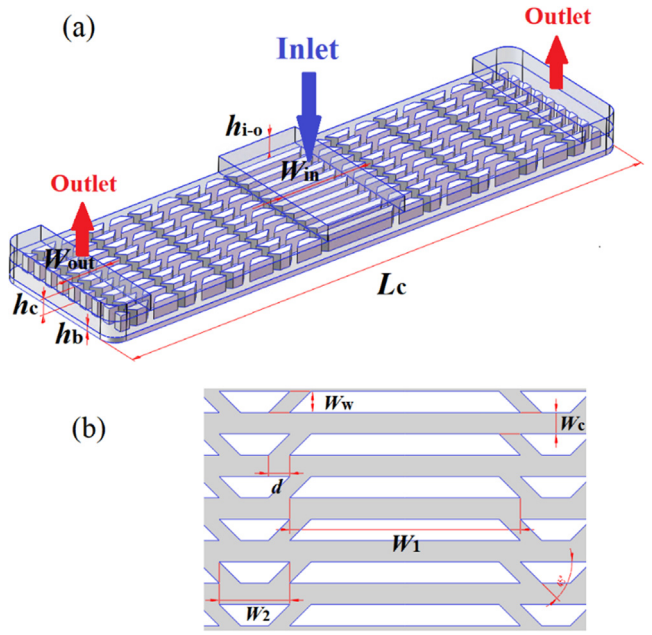

Fig. 1. (a) Schematic diagram and (b) geometric parameters of the MMC-SOC heat sink.

efficiency comparing with Newtonian fluid. Drummond et al. [33] fabricated a hierarchical MMC heat sink imbedded directly into the heated substrate to reduce thermal resistances for two-phase cooling experiments. In their study, a heat sink with 15 μm × 300 μm channels can dissipate 910 W/cm^2 with temperature rise of less than 47 °C above the fluid inlet temperature and pressure drop less than 162 kPa, the engineered dielectric liquid HFE-7100 as the working fluid. A summary of selected manifold-microchannel (MMC) literature review is shown in Table 1.

Secondary flow is another promising heat transfer enhancement technique, which can promote fluid mixing and decrease the thermal boundary layer thickness. Steinke and Kandlikar [34] pointed out that smaller channels between the main flow channels could be added between the main flow channels by using offset strip fins or a venture. Secondary flow will move from one main channel to another via these smaller channels, which can enhance the thermal performance of a micro-channel heat exchanger. They also pointed out that the pressure drop penalties could be a limiting factor for secondary flow devices. Lee et al. [35] proposed the concept of sectional oblique fins, and smaller oblique channels were added into the main flow in microchannels. Compared with the conventional microchannel heat sink, the heat transfer enhancement could reach 2.2 when the Reynolds number exceeds 600, which is caused by the combined effects of thermal boundary layer redeveloping and the secondary flows. They also fabricated microchannel heat sinks with oblique fins using a square copper block of dimensions 25 mm × 25 mm × 70 mm and carried out experimental study with single-phase water as working fluid. Their results show that the pressure drop penalty is negligible when Re is less than 400 for modified microchannel heat sink with a 500 μm nominal channel width. Kuppusamy et al. [36] introduced alternating slanted passages in microchannel to induce secondary flow and carried out numerical studies on the flow and thermal performance of the proposed microchannel heat sinks. Comparing with straight channel heat sink, the proposed microchannel heat sink was shown to increases the overall performance by 146% and reduces thermal resistance by 23.2%. In addition, they found that the thermal enhancement comes together with a 6% reduction in pressure drop, which has multiplied the benefits of secondary channels. Ghani et al. [37] proposed a hybrid design using rectangular ribs and secondary channels in alternating orientation. The effects of geometrical parameters, including relative width of secondary channel, relative rib width and angle of secondary channel, on the flow and thermal performance were investigated numerically. The secondary channels can provide more flow area which reduces the pressure drop, and the rectangular ribs force more flow towards secondary channels which increases the flow exchange between adjacent channels. The performance factor PEC was 1.98 at Re = 500 for the best hybrid heat sink.

We can see that both the manifold arrangement and secondary flow can enhance the thermal performance of microchannel heat sink. To our best knowledge, however, no investigation has been done on combining these two cooling techniques. Therefore, the aim of the present study is to present a new hybrid design that uses the manifold arrangement to reduce the effective fluid flow length and the corresponding pressure drop. Besides, the secondary channels can enhance the thermal performance by combined effects of promoting fluid mixing and decreasing the thermal boundary layer thickness. In order to find the optimum geometric parameters, two variables, the secondary channel width d and the longer-edge length W_1 of the fins located at the inlet, are designed. A total of 21 types of heat sinks are obtained by changing d and W_1, and fully three-dimensional (3D) conjugate heat transfer analyses are performed to study the fluid flow and heat transfer characteristics under different Reynolds numbers. A region named Design Optimization Area (DOA) is defined, where ΔP and R_t can be both reduced. The simulation results show that most of the designed hybrid heat sinks are in the region of DOA at Re = 295, suggesting that the thermal enhancement comes together with the pressure drop reduction. In addition, by changing the velocity inlet boundary condition to pressure inlet boundary condition, we find that the heat sink with geometrical parameters of (λ = 1, β = 1) yields the best overall performance among those proposed heat sink designs at Re = 295.

2. Modelling of microchannel heat sink

Fig. 1 illustrates the computational domain with geometrical parameters for both of secondary oblique channels and manifold arrangement. Fully 3D conjugate heat transfer analyses are performed to study the heat removal capacity of the proposed microchannel heat sink with manifold arrangement and secondary oblique channels (MMC-SOC). As shown in Fig. 1, there are ten microchannels in the microchannel heat sink etched into a 400 μm-thick silicon and the flow enters the microchannels from the manifold inlet channel (located at the center position), then splits and flows through the microchannels, and finally exits to the two manifold outlet channels (located at both ends of the microchannel). The total channel length L_c, manifold inlet/outlet widths W_{in} and W_{out} are 10.6 mm, 1.6 mm and 0.8 mm, respectively. The height and width of the microchannel are h_c = 300 μm and W_c = 150 μm, respectively. The width of the channel wall W_w equals to channel width W_c. The longer-edge length of the fins except those located at the inlet is W_2 = 500 μm. The heights of the base and inlet/outlet are h_b = 100 μm and h_{i-o} = 300 μm, respectively.

In order to study the impact of secondary channels and manifold arrangement on the flow and thermal performance of the heat sink, the secondary channel width d and the longer-edge length W_1 of the fins located at the inlet are selected as the variables. We also define two dimensionless numbers: the relative secondary channel width λ and the relative longer-edge length β. The relative secondary channel width λ is defined as the ratio of secondary channel width d to the main channel width W_c, i.e. $\lambda = d/W_c$, while the relative longer-edge length β is defined as the ratio of the longer-edge length W_1 of the fins located at the inlet to the manifold inlet width W_{in}, i.e. $\beta = W_1/W_{in}$. Twenty-one types of heat sinks are designed by changing the secondary channel width d and the longer-edge length W_1. The secondary channel width d are 100, 150, 225, 300, 375 μm and the corresponding λ are respectively 0.666, 1, 1.5, 2, 2.5. In addition, the longer-edge length W_1 are 400, 500, 800, 1600, 2400, 3200 μm and the corresponding β are

respectively 0.25, 0.313, 0.5, 1, 1.5, 2.

3. Numerical method

Finite volume method is utilized to discretize the governing equation. The SIMPLE algorithm is adopted to accomplish the pressure-velocity coupling. At the same time, the second order upwind scheme is used for convective term and second order central difference scheme is applied for diffusion term. Furthermore, convergence criterions are set to be less than 10^{-6} for continuity and less than 10^{-9} for energy. The computational fluid dynamic (CFD) software FLUENT 14 is used to solve the three-dimensional heat transfer and fluid flow equations according to the following assumptions:

(i) The flow is laminar, incompressible and Newtonian.
(ii) The fluid flow and heat transfer are all in steady-state and three-dimensional.
(iii) The thermophysical properties of both fluid and heat sink material are constant.
(iv) Neglecting the viscous dissipation and the radiation heat transfer (the maximum Brinkman number in our study is less than 0.005).

3.1. Governing equations

Based on the above assumptions, the governing equations of mass, momentum and energy can be written as follows:

Continuity equation:

$$\frac{\partial u}{\partial x}+\frac{\partial v}{\partial y}+\frac{\partial w}{\partial z}=0 \tag{1}$$

Momentum equations:

$$u\frac{\partial u}{\partial x}+v\frac{\partial u}{\partial y}+w\frac{\partial u}{\partial z}=-\frac{1}{\rho_f}\frac{\partial p}{\partial x}+\frac{\mu_f}{\rho_f}\left(\frac{\partial^2 u}{\partial x^2}+\frac{\partial^2 u}{\partial y^2}+\frac{\partial^2 u}{\partial z^2}\right) \tag{2}$$

$$u\frac{\partial v}{\partial x}+v\frac{\partial v}{\partial y}+w\frac{\partial v}{\partial z}=-\frac{1}{\rho_f}\frac{\partial p}{\partial y}+\frac{\mu_f}{\rho_f}\left(\frac{\partial^2 v}{\partial x^2}+\frac{\partial^2 v}{\partial y^2}+\frac{\partial^2 v}{\partial z^2}\right) \tag{3}$$

$$u\frac{\partial w}{\partial x}+v\frac{\partial w}{\partial y}+w\frac{\partial w}{\partial z}=-\frac{1}{\rho_f}\frac{\partial p}{\partial z}+\frac{\mu_f}{\rho_f}\left(\frac{\partial^2 w}{\partial x^2}+\frac{\partial^2 w}{\partial y^2}+\frac{\partial^2 w}{\partial z^2}\right) \tag{4}$$

Energy equation for the coolant:

$$u\frac{\partial T_f}{\partial x}+v\frac{\partial T_f}{\partial y}+w\frac{\partial T_f}{\partial z}=\frac{k_f}{\rho_f C_{pf}}\left(\frac{\partial^2 T_f}{\partial x^2}+\frac{\partial^2 T_f}{\partial y^2}+\frac{\partial^2 T_f}{\partial z^2}\right) \tag{5}$$

Energy equation for the heat sink solid region:

$$k_s\left(\frac{\partial^2 T_s}{\partial x^2}+\frac{\partial^2 T_s}{\partial y^2}+\frac{\partial^2 T_s}{\partial z^2}\right)=0 \tag{6}$$

where ρ_f is the density of the fluid, μ_f is the viscosity of the fluid, k_f and C_{pf} are the thermal conductivity and specific heat capacity of the fluid respectively, k_s is the thermal conductivity of the solid.

3.2. Boundary conditions and physical properties of materials

A uniform heat flux q'' of 200 W/cm^2 is applied to the backside of the heat sink (heat source). Water is used as the cooling fluid. Velocity inlet boundary condition is imposed and the inlet velocity is calculated from the volume flow rate $\dot{V}$. The volume flow rate in the heat sink is chosen in the range of 0.04–0.28 L/min and the corresponding Reynolds number ranges from 147 to 885. The inlet temperature of the coolant is set as room temperature 293.15 K (20 °C). In all cases, pressure boundary condition is assigned to the outlet and the pressure at the outlet is assumed to be zero. No-slip and no-penetration boundary conditions are applied at the interior walls of the heat sink. Adiabatic wall conditions are applied to all external boundaries of the heat sink except the backside.

In this study, deionized water (DI water) is used as the coolant and silicon is used as the solid material. The properties, including the density ρ, dynamic viscosity μ, thermal conductivity k and specific heat capacity C_p, of water and silicon are selected based on the room temperature 293.15 K (20 °C).

3.3. Grid independence and CFD simulation

In order to ensure the numerical results are independent of the mesh structure, a grid independence study is conducted. The STAR-CCM + software is used to generate three dimensional polyhedral with prism layer mesh near liquid–solid interface. Fig. 2 shows the three-dimensional polyhedral with prism layer mesh structure of a hybrid microchannel heat sink with geometrical parameters of ($\lambda = 1$, $\beta = 1$).

The grid number of the MMC-SOC heat sink varies from 0.45 million to 3.81 million for Reynolds number of 295 ($\dot{V}$ = 0.08 L/min). The effects of grid number on the Nusselt number Nu and pressure drop ΔP are

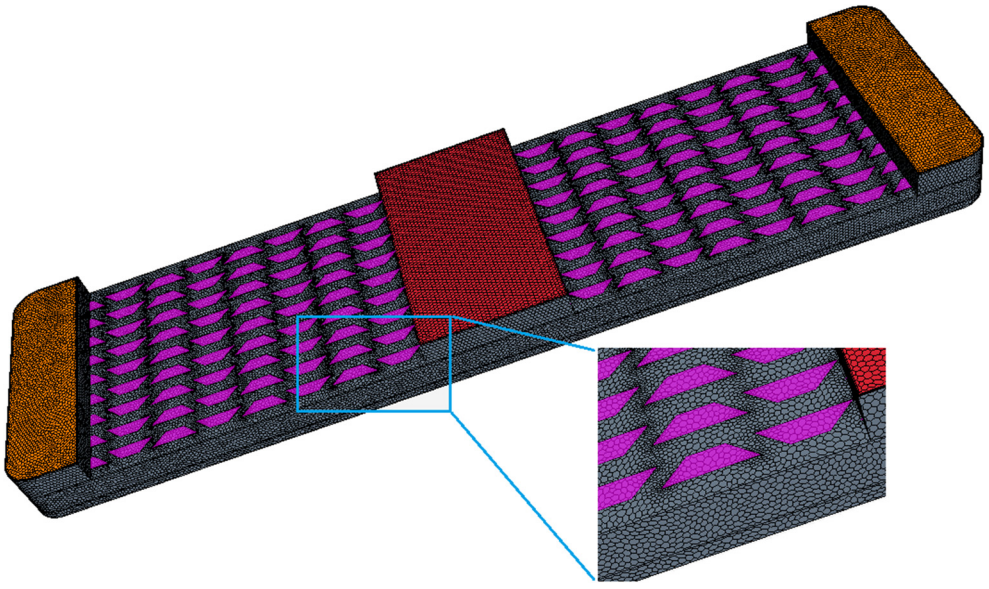

Fig. 2. Three-dimensional polyhedral with prism layer mesh structure of the hybrid heat sink with geometrical parameters of ($\lambda = 1$, $\beta = 1$).

studied numerically. The relative errors E% for Nu and ΔP of different grids in comparison to the finest grids of 3.81 million are shown in Table 2. Compared with other mesh sizes, the relative errors of a grid of 2.75 million cells can be neglected. We also conduct grid independence study at the highest Reynolds number (Re = 885) and find that the relative errors for Nu and ΔP of 2.75 million cells are respectively 1.23% and 0.43%, which indicates that the mesh system with 2.75 million cells is adequately fine over the full range of Re in this study. Therefore, considering both accuracy and efficiency, the grid system with 2.75 million cells is used in our numerical simulations.

3.4. Validation of rectangular microchannel (RC)

To verify the accuracy and reliability of the present numerical simulation, the numerical results of rectangular microchannel model on the thermal and hydraulic performance are compared with experimental results of Qu and Mudawar [8]. In Qu and Mudawar's work, four thermocouples were used to measure the temperature distribution inside the heat sink. Here we define the average value of those four temperatures as the average temperature T_{ave} at the corresponding wall (z = 3175 μm). The comparisons of pressure drop and average temperature between the current simulation results and the experimental data at heat flux of 100 W/cm^2 and 200 W/cm^2 are shown in Fig. 3(a) and (b), respectively. It is clear that both the numerical predicted pressure drop and average temperature are in good agreement with experimental data, demonstrating the accuracy of the numerical scheme used in this study.

3.5. Data reduction

This section presents the relevant expressions that are used to characterize the heat transfer and fluid flow performance in MMC-SOC heat sink.

1) The Reynolds number is expressed as follows

$$Re = \frac{\rho u_m D_h}{\mu} \tag{7}$$

where D_h represents the hydraulic diameter D_h is calculated as

$$D_h = \frac{2W_c h_c}{W_c + h_c} \tag{8}$$

where ρ, u_m and μ are density, mean velocity and dynamic viscosity of the working fluid, respectively. h_c and W_c are the height and width of the microchannel.

2) The total thermal resistance

$$R_t = \frac{\Delta T_{max}}{Q} = \frac{T_{max} - T_{in}}{Q} \tag{9}$$

where T_{max} and T_{in} are the maximum temperature of the microchannel heat sink base and the fluid temperature at the inlet, respectively. Q is the total heat flux applied to the backside of the heat sink and is defined as $Q = q'' \times A_{hs}$, where A_{hs} is the area of the heat source, i.e. the area of the microchannel heat sink backside.

3) The average heat transfer coefficient is given by

$$h = \frac{q \times A_{hs}}{A_{con} \times \Delta T} = \frac{Q}{A_{con} \times \Delta T_{m,loc}} \tag{10}$$

$$\Delta T_{m,loc} = \frac{\Delta T_{max} - \Delta T_{min}}{\ln\left(\frac{\Delta T_{max}}{\Delta T_{min}}\right)} = \frac{(T_w - T_{in}) - (T_w - T_{out})}{\ln\left[\frac{(T_w - T_{in})}{(T_w - T_{out})}\right]} \tag{11}$$

where A_{con} is the area of the convective heat transfer. T_{out} is the area-weighted average temperature of fluid at the outlet. T_w is the area-weighted average temperature of the interface between the coolant and solid wall.

4) The average Nusselt number is given by

$$Nu_{ave} = \frac{h_{ave} D_h}{k_f} \tag{12}$$

where k_f is the thermal conductivity of the working fluid.

5) The apparent Darcy friction factor in rectangular channel is given by

$$f = \frac{2\Delta P D_h}{L_t \rho u_m^2} \tag{13}$$

where L_t is the total flow length, which is half of the total channel length L_c.

6) The overall performance of heat sinks is evaluated using performance evaluation criteria, which is expressed as follows

$$PEC = \frac{Nu/Nu_0}{(f/f_0)^{1/3}} \tag{14}$$

where Nu_0 and f_0 represent the Nusselt number and Darcy friction factor in the original MMC heat sink respectively.

4. Results and discussion

The ANSYS Fluent 14.0 software is used to simulate the flow and heat transfer characteristics of the twenty-one types of hybrid heat sinks with manifold arrangement and secondary oblique channels. Firstly, the common MMC heat sink and hybrid heat sinks are studied by 3D numerical simulations at Re = 295 ($\dot{V}$ = 0.08 L/min). Then, a careful comparison is made to illustrate the effective flow and thermal performance of the proposed hybrid MMC-SOC heat sink. We discuss the relevance of the current performance evaluation method and make an attempt to find out the best heat sink structure. Moreover, some parameters, such as pressure drop ΔP and total thermal resistance R_t, are examined in detail with the Reynolds numbers ranging from 147 to 885 (the corresponding inlet volume flow rates $\dot{V}$ are 0.04, 0.08, 0.12, 0.16, 0.20 and 0.24 L/min).

4.1. Average flow and heat transfer characteristics

The parameters, such as the maximum temperature of the heat source T_{max}, the outlet pressure P_{out} and the outlet temperature T_{out}, are extracted from numerical results, and are used to calculate the pressure drop ΔP, the total thermal resistance R_t, the heat transfer coefficient h, the average Nusselt number Nu, the Darcy friction factor f and the performance evaluation criteria PEC. In addition, the pumping power P_p is expressed in terms of the product of the pressure drop ΔP and the fluid volume flow rate $\dot{V}$, i.e. $P_p = \dot{V} \times \Delta P$. It is important to note that we don't distinguish between static pressure drop and total pressure drop when calculating the pumping power P_p due to the negligible difference between the total pressure and static pressure. In this study, the performance of those designed twenty-one heat sinks are studied under the same fluid volume flow rate $\dot{V}$, so the pressure drop ΔP can represent the pumping power P_p. Those relevant numerical results that

Table 2
Grid independence test.

Grid Numbers × 10^6	Nu	E%	ΔP (Pa)	E%
0.45	12.077	12.82	7931	1.08
1.06	11.425	6.76	7944	1.25
2.75	10.813	1.04	7927	1.03
3.81	10.702	–	7846	–

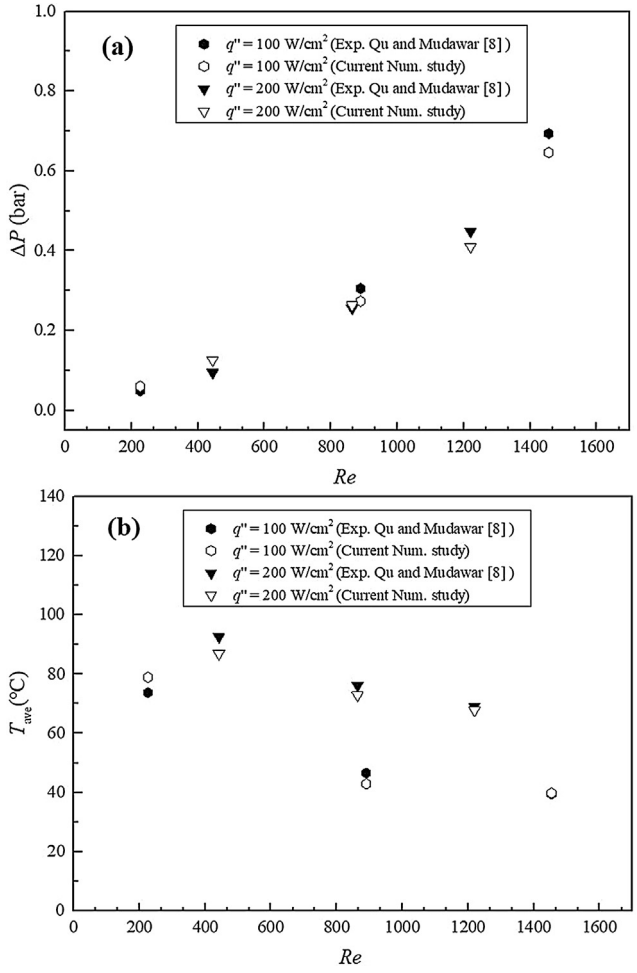

Fig. 3. Comparisons of (a) pressure drop, (b) average temperature at the heat sink wall (z = 3175 μm) with experimental data of Qu and Mudawar [8].

can characterize the thermal and flow performance are listed in Table 3.

As shown in Table 3, the total thermal resistances R_t, or the maximum temperature T_{max}, of all hybrid heat sinks are lower than that of the original MMC heat sink, indicating a better thermal performance. However, when considering the pressure drop ΔP, or the pumping power P_p, only a portion of the hybrid heat sinks perform better than the MMC heat sink. Therefore, different hybrid heat sinks with best performance can be defined based on different perspectives. If we focus on R_t, the heat sink with geometrical parameters of ($\lambda = 1$, $\beta = 1$) shows the best performance. The T_{max} and R_t of this heat sink are 335.85 K and 0.7085 K/W, respectively, both lower than those of other heat sinks. From the perspective of performance evaluation criteria *PEC*, which combines the Nusselt number *Nu* together with Darcy friction factor *f*, the heat sink with geometrical parameters of ($\lambda = 2.5$, $\beta = 1$) shows the best performance with the highest *PEC* of 1.3843 and the lowest pressure drop. However, when both the pressure drop and thermal resistance are taken into account, the heat sink with geometrical parameters of ($\lambda = 2$, $\beta = 1$) may be the best one because it has relatively small maximum temperature T_{max} and pressure drop ΔP. The value of ΔP of this heat sink is 7611 Pa, about 4% lower than the heat sink ($\lambda = 1$, $\beta = 1$).

The above analyses indicate that the existing evaluation method (*Nu*, *f*, *PEC* etc.) may be inapplicable for the performance evaluation of microchannel heat sink geometric optimization. This is because there's no need to take into account the value of the convective heat transfer area A_{con}. Actually, our numerical results have demonstrated that larger convective heat transfer area doesn't mean better thermal performance. As is known, the key purpose of the novel cooling strategy is to ensure the heat source (electronic devices) work at reasonable temperature with the lowest possible pumping power P_p. In other words, the cooling strategy should maintain low R_t with the lowest possible P_p. Therefore, R_t and P_p are two essential parameters which are necessary to be considered, which agrees with the understanding of some researchers [38,39]. Xie et al. [38] and Chai et al. [39] used the relationship between R_t and P_p to comprehensively assess the performance of microchannel heat sink. It is a beneficial attempt for finding out a more reasonable evaluation method.

Fig. 4 shows the relationship between the total thermal resistance R_t and the pressure drop ΔP for all the twenty-one heat sinks at Re = 295 ($\dot{V}$ = 0.08 L/min). For heat sink with $\lambda = 0.666$, increasing ΔP will

Table 3
Overall performance of the twenty-one types of heat sinks at Re = 295 ($\dot{V}$ = 0.08 L/min).

λ	β	T_{max} (K)	ΔP (Pa)	R_t (K/W)	h (W/m²K)	Nu	f	PEC
0.666	0.3125	337.43	8084	0.7347	30,830	10.277	0.2785	1.1834
	1	336.70	8041	0.7226	30,967	10.322	0.2770	1.1908
	1.5	336.68	8408	0.7223	30,700	10.233	0.2896	1.1631
	2	337.21	8269	0.7311	30,135	10.045	0.2849	1.1481
1	0.25	336.80	7818	0.7243	32,193	10.731	0.2693	1.2496
	0.3125	336.39	7805	0.7175	32,200	10.733	0.2689	1.2506
	1	335.85	7927	0.7085	32,437	10.812	0.2731	1.2533
	2	338.06	8095	0.7452	31,309	10.436	0.2789	1.2013
1.5	0.3125	343.42	7814	0.8341	33,842	11.281	0.2692	1.3139
	1	343.22	7798	0.8308	33,801	11.267	0.2686	1.3131
	2	339.83	7829	0.7746	32,166	10.722	0.2697	1.2480
2	0.3125	343.21	8009	0.8307	35,288	11.763	0.2759	1.3588
	0.5	342.13	7781	0.8127	33,931	11.310	0.2680	1.3192
	1	336.86	7611	0.7253	34,028	11.343	0.2622	1.3327
	1.5	339.75	7832	0.7732	33,962	11.321	0.2698	1.3175
	2	343.28	8102	0.8318	32,734	10.911	0.2791	1.2556
2.5	0.3125	339.52	7848	0.7694	35,487	11.829	0.2704	1.3757
	0.5	346.14	7612	0.8793	34,694	11.565	0.2622	1.3587
	1	340.69	6894	0.7888	34,199	11.400	0.2375	1.3843
	1.5	343.77	8145	0.8400	34,896	11.632	0.2806	1.3361
	2	339.77	7548	0.7736	33,107	11.036	0.2600	1.3002
MMC		345.96	8082	0.8763	26,050	8.683	0.2784	–

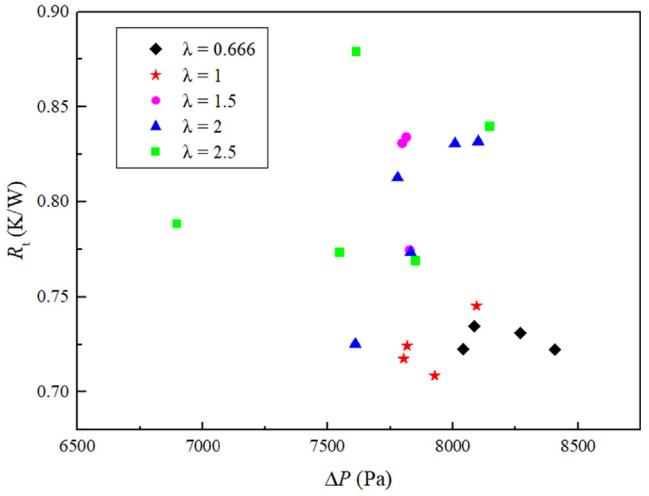

Fig. 4. The total thermal resistance R_t as a function of the pressure drop ΔP for all the twenty-one heat sinks at Re = 295.

cause R_t to increase firstly and then decrease; For heat sink with $\lambda = 1$, R_t generally increases with increasing ΔP; For heat sink with $\lambda = 1.5$, ΔP shows little variation while R_t varies greatly for different structures; For heat sink with $\lambda = 2$, R_t generally increases with increasing ΔP, which indicates that the decrease of R_t and ΔP can be obtained simultaneously; For heat sink with $\lambda = 2.5$, a clear relationship between R_t and ΔP is not seen. Moreover, as can be seen from Fig. 4, there seems to be a tendency that numerical data points of designed heat sinks gradually move from the upper left corner to the lower right corner with the decrease of the the relative secondary channel width λ. This tendency demonstrates that as the value of d decreases, the thermal resistance R_t becomes smaller while the pressure drop ΔP becomes larger, indicating a better heat transfer performance and a worse flow performance. In order to verify this conjecture, the trend of R_t and ΔP with variation of λ while β constrained at 2 is plotted in Fig. 5. Unfortunately, there is no definite relationship between R_t and λ, or ΔP and λ. However, there actually exists a tendency between the numerical data points and λ in Fig. 4, where the geometrical parameters have a great impact on the thermal and hydraulic performance of the proposed heat sink. We will continue this discussion in the following sections.

In addition, in order to provide a careful comparison between the proposed MMC-SOC and original MMC heat sinks, the thermal resistance R_t and pressure drop ΔP are dealt with dimensionless method. The normalized improvement factors of both thermal and hydraulic performance are presented in Fig. 6. The abscissa is pressure drop ratio ($\Delta P/\Delta P_0$), and the ordinate is the total thermal resistance ratio (R_t/R_{t0}). Here, the subscript 0 denotes the performance of the traditional MMC heat sink. If the value of ($\Delta P/\Delta P_0$) is less than 1, pressure drop reduction can be obtained compared with MMC heat sink. Similarly, if the value of (R_t/R_{t0}) is less than 1, better heat transfer performance can be obtained.

The shadow region in Fig. 6 illustrates the area where the values of (R_t/R_{t0}) and ($\Delta P/\Delta P_0$) are both less than 1. In this area, with the introduction of the secondary channels, the thermal performance enhancement comes together with the pressure drop reduction compared to the original one. We define this shadow region as Design Optimization Area (DOA). It is well known that improving the heat transfer performance while in the meantime, reducing the pressure drop is always a challenging task. Fortunately, as seen in Fig. 6, most of the designed hybrid heat sinks are in the region of DOA, suggesting that the thermal enhancement comes together with the pressure drop reduction for most heat sinks.

Although the Design Optimization Area can be obtained through the relationship between (R_t/R_{t0}) and ($\Delta P/\Delta P_0$), it is also difficult to find out the best heat sink. For the data shown in Fig. 6, for example, there are three circles and represent the heat structures with geometrical parameters of ($\lambda = 2.5$, $\beta = 1$), ($\lambda = 2$, $\beta = 1$) and ($\lambda = 1$, $\beta = 1$) from left to right, respectively. We have pointed out that those three heat sinks all might be the best one depending on the perspectives. The total thermal resistance R_t of heat sink ($\lambda = 1$, $\beta = 1$) is lower than others. The heat sink ($\lambda = 2$, $\beta = 1$) has relatively small thermal resistance R_t and pressure drop ΔP. And, the structure ($\lambda = 2.5$, $\beta = 1$) has the highest PEC and lowest pressure drop. We define those three heat structures as 1#, 2# and 3# heat sinks from left to right, as shown in Fig. 6. The above analyses demonstrate that it is difficult to find out the best heat sink structure only through Fig. 6. To solve this problem, we change the velocity inlet boundary condition to pressure inlet boundary condition. The simulation results, i.e. the pumping power P_p and (R_t/R_{t0}), at given inlet pressure (7611 Pa) are listed in Table 4. The fluid volume flow rate of 3# heat sink is 1.28×10^{-6} m^3/s, which is smaller than the other two heat sinks, indicating the P_p of 3# heat sink is the minimum one. In addition, the value of (R_t/R_{t0}) of 3# heat sink is 0.8062, which is also the minimum one, indicating that this structure has the best heat transfer performance. Consequently, 3# heat sink yields the best overall performance, while 1# heat sink shows the worst performance. This result suggests that when the secondary channel width d equals to the main channel width W_c, and the longer-edge length of the fins W_1 equals to the manifold inlet width W_{in}, the heat sink can achieve the best overall performance. At a Reynolds number of 295, 3# heat sink can reduce the pressure drop ΔP by 1.91% and simultaneously decrease the total thermal resistance R_t by 19.15% compared to the original MMC heat sink.

Fig. 7 displays the temperature distribution contours of the original MMC and 3# heat sinks at Re = 295 ($\dot{V}$ = 0.08 L/min), including the temperature contours at different cross sections and the heat source (backside of heat sink). As can be seen from Fig. 7, the high temperature region for all heat sinks locates at the edge of the outlet due to the low heat transfer coefficient, while the low temperature region occurs in the entrance region, due to the entrance effects and jet impingement. The maximum temperatures of these two heat sinks are 345.95 K and 335.84 K, respectively. The heat is conducted from the heat source to the base and fins, and then transferred from channel wall into the cooling fluid by convection. The temperature gradient develops in the thermal boundary layer and grows along coolant flowing downstream. As presented in Fig. 7(a) and (b), the temperature gradient near the channel wall changes significantly and the water temperature at the central portion of the channel is almost constant. In addition, the cooling fluid temperatures become higher and higher along the flow direction due to the absorption of heat from the surrounding channel walls. Compared with the original MMC heat sink, the hybrid heat sink can promote fluid mixing and decrease the thermal boundary layer

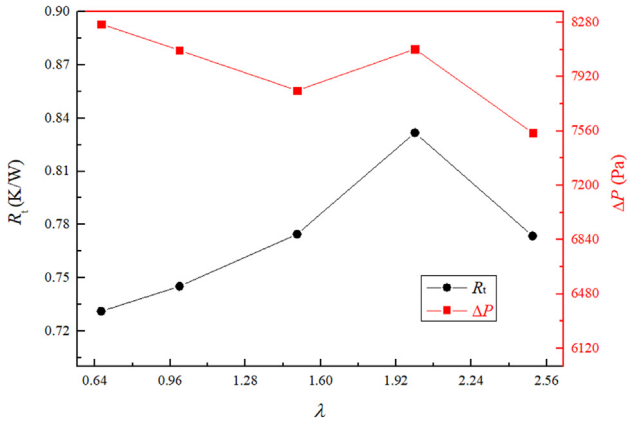

Fig. 5. Variation of R_t and ΔP with λ at Re = 295.

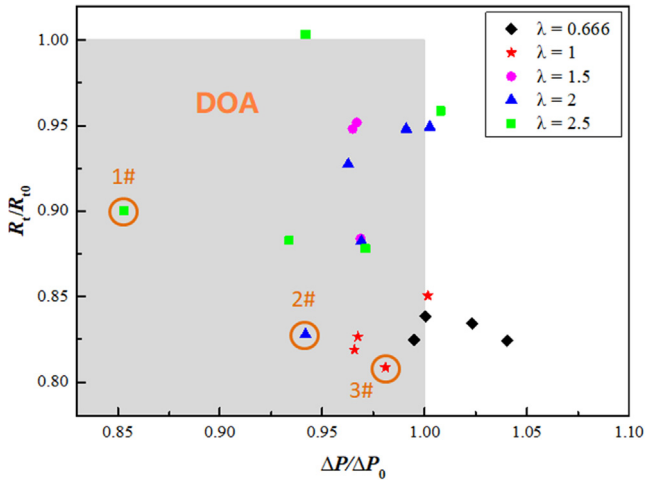

Fig. 6. The relationship between thermal resistance ratio (R_t/R_{t0}) and pressure drop ratio ($\Delta P/\Delta P_0$) for all the twenty-one heat sinks at Re = 295.

Table 4
Numerical results of 1#, 2# and 3# heat sinks at given pressure drop.

	$\dot{V}$ (m^3/s) × 10^{-6}	(R_t/R_{t0})	P_p ($\dot{V}\Delta P$)	(R_t/R_{t0})
1#	1.41	0.8728	High	High
2#	1.32	0.8135	Medium	Medium
3#	1.28	0.8062	Low	Low

thickness due to the introduction of secondary channels, which can enhance the heat transfer performance. Consequently, it is clearly shown that the temperature gradient between the coolant and the fin of 3# heat sink is lower than the MMC heat sink. In addition, better surface temperature uniformity of 3# heat sink can be observed.

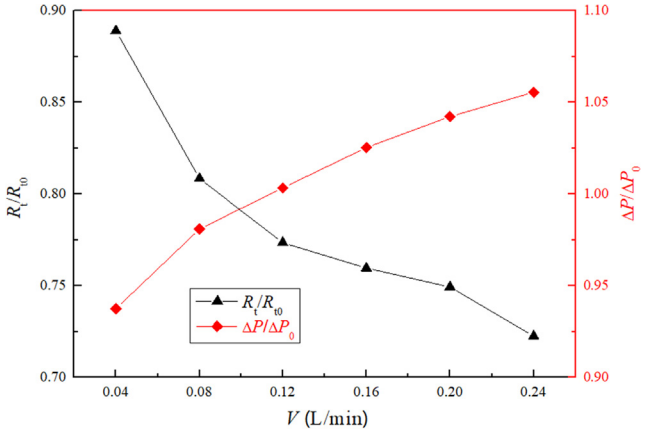

Fig. 8. Comparisons of thermal-hydraulic performance between the best heat sink and the original MMC heat sink at different volume flow rates.

4.2. Effects of volume flow rate and geometrical parameters

Fig. 8 shows the thermal and hydraulic performance of the best heat sink with specific geometrical parameters of (λ = 1, β = 1) at different volume flow rates ranging from 0.04 L/min to 0.24 L/min, with Reynolds numbers from 147 to 885. As the volume flow rate $\dot{V}$ increases, the thermal resistance ratio (R_t/R_{t0}) becomes smaller and the pressure drop ratio ($\Delta P/\Delta P_0$) becomes larger, as shown in Fig. 8. This tendency indicates that larger volume flow rate can force more fluid to flow through secondary channels, which can further promote fluid mixing and decrease the thermal boundary layer thickness. Consequently, the ratio (R_t/R_{t0}) decreases with increasing the volume flow rate and better thermal performance can be obtained. However, the enhancement of fluid velocity and mixing also bring higher pressure drop penalty. When $\dot{V}$ increases beyond 0.12 L/min (Re = 442), the value of ($\Delta P/\Delta P_0$) exceeds 1, indicating the designed heat sink has a larger pressure drop compared with the original MMC heat sink. Similar tendency has also been reported by Lee et al. [35]. They fabricated microchannel heat

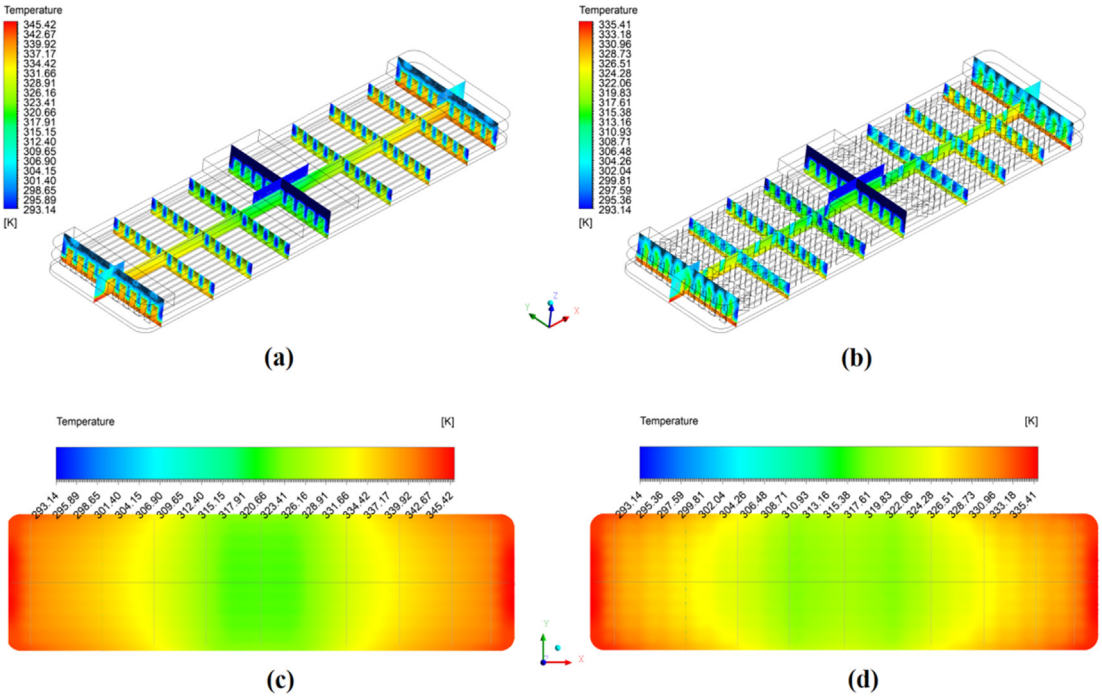

Fig. 7. Temperature distribution contours for the (a) and (c) original MMC heat sink, and (b) and (d) 3# heat sink at Re = 295 ($\dot{V}$ = 0.08 L/min). (a) and (b) are the temperature contours of heat sink at different cross sections while (c) and (d) are temperature contours of the heat source.

sink with oblique fins and found that the pressure drop penalty is negligible only when *Re* is less than 400. The above results suggest that the effects of secondary channels on the pressure drop are related to both the geometrical parameters and the Reynolds numbers. A certain hybrid structure heat sink can reduce the pressure loss at low Reynolds numbers, but it may increase the pressure loss at high Reynolds numbers. In addition, as shown in Fig. 7, the pressure drop ratio ($\Delta P/\Delta P_0$) of the best heat sink becomes larger than 1 when the volume flow rate $\dot{V}$ increases beyond 0.12 L/min, which makes the best heat sink structure leave DOA.

Fig. 9 shows the effect of Reynolds number (or the volume flow rate) on the relationship between the normalized R_t and ΔP for all the twenty-one heat sinks. From Fig. 9, we can conclude that:

i) As *Re* increases, all numerical data points gradually move from the upper left corner to the lower right corner, which demonstrates that as *Re* increases, the normalized value of R_t becomes smaller while the normalized value of ΔP becomes larger. In other words, the heat transfer performance becomes better while the hydraulic performance becomes worse when increasing Reynolds number. For example, the values of (R_t/R_{t0}) and ($\Delta P/\Delta P_0$) are 0.8891 and 0.9374 for 3# heat sink at $Re = 147$, respectively. However, these two values become 0.7225 and 1.0556 when *Re* increases to 885.

ii) As can be seen in Fig. 9, the number of data points outside DOA are 3, 4, 13, 20, 21 at $Re = 147$, 295, 442, 590 and 885, respectively. It is obvious that the number of data points outside DOA increases with the increase of *Re*, indicating that the number of heat sink structures can enhance the thermal and hydraulic performance simultaneously decreases. For the data shown in Fig. 9, for example, the pressure drop ratio ($\Delta P/\Delta P_0$) of 3# heat sink is larger than 1 when the Reynolds number increases beyond 412, which causes the best heat sink structure to leave DOA. In addition, as shown in Fig. 9(f), all data points have left DOA when *Re* increases to 885.

iii) As *Re* increases, greater dispersion of data points has been observed. This dispersion reflects the dependence of the numerical results on the heat sink structures. Greater dispersion, i.e. larger *Re*, indicates that the dependence of the thermal and hydraulic performance on the heat sink structure becomes weaker. In addition, as mentioned in ii), the number of heat sinks in DOA decreases with increasing *Re*. Therefore, at small *Re*, the dispersion of data points is small and the number of heat sinks in DOA is large, which makes it easier to find out those heat sink structures that can enhance the overall performance compared with the original MMC heat sink. However, it will take more time to find those better heat sink structures when the Reynolds number is large.

iv) With the increase of *Re*, data points outside DOA may move into the region. As shown in Fig. 9(a), for example, it is obvious that there are two data points (i.e. two heat sink structures) outside DOA with $\lambda = 2$ at $Re = 147$. However, as shown in Fig. 9(b), these two data points have moved into DOA when *Re* increases to 295. Above numerical results demonstrate that both the geometrical parameters and Reynolds numbers all have an important impact on the overall performance of secondary channels. A certain hybrid structure heat sink could perform better than the original MMC heat sink at low Reynolds numbers, while it may perform worse at high Reynolds numbers.

4.3. Thermal and hydraulic characteristics

In order to better understand the existing fluid flow and the heat transfer phenomena in the MMC-SOC heat sink, the secondary flow field, including the flow velocity magnitude distribution, velocity vectors and flow streamlines is analyzed in detail. Fig. 10(a) illustrates the flow velocity magnitude distribution around the oblique fins on x-y plane ($z = 0.25$ mm) at $Re = 295$. The maximum flow velocity is located at the middle region of the microchannel, while the minimum velocity is found in the vortices region. Vortices are periodically generated in the secondary channels due to the introduction of secondary oblique channels, as shown in Fig. 10(b). It is obvious that some coolant flows through the secondary channels and fluid vortices are generated when the flowing coolant encounters interruptions, which enhances the fluid mixing. The breakage of the continuous fin is obtained by using oblique fins, which brings the disruption of both the hydrodynamic and thermal boundary layer. In addition, the development of boundary

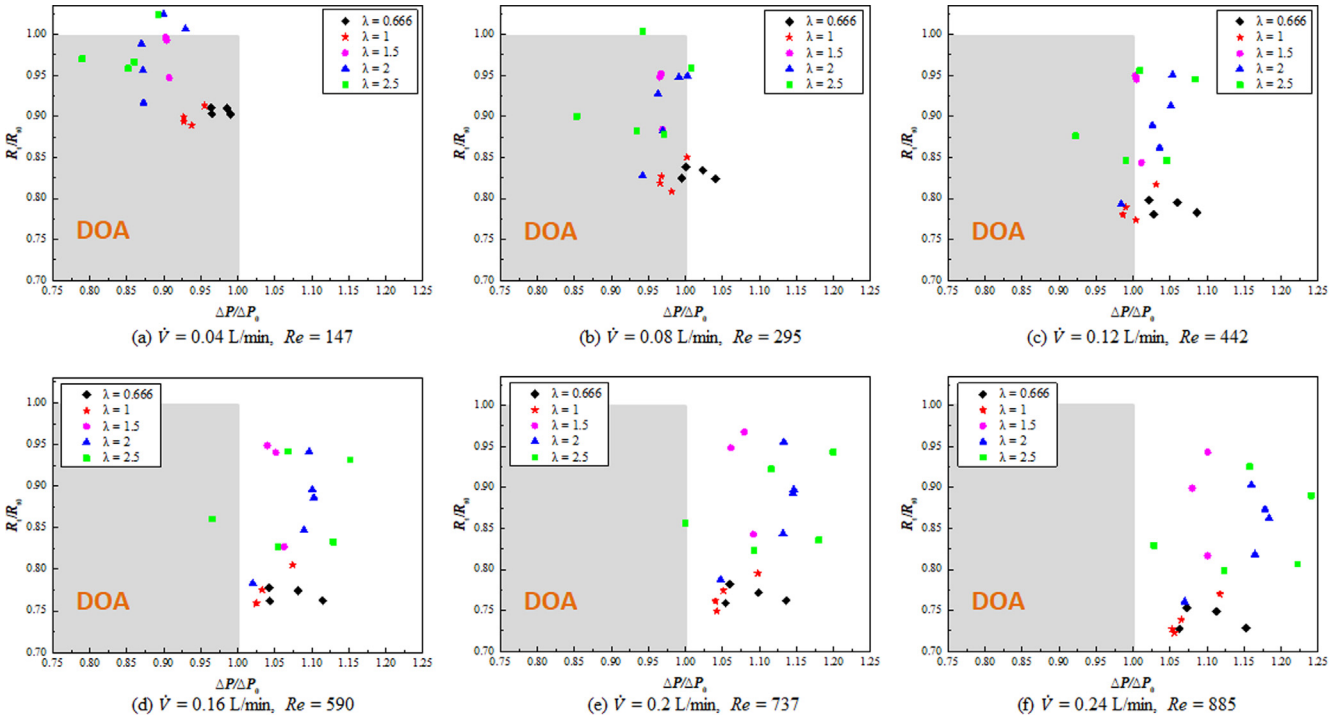

Fig. 9. Effects of Reynolds number on the relationship between (R_t/R_{t0}) and ($\Delta P/\Delta P_0$) for all the twenty-one types of heat sinks.

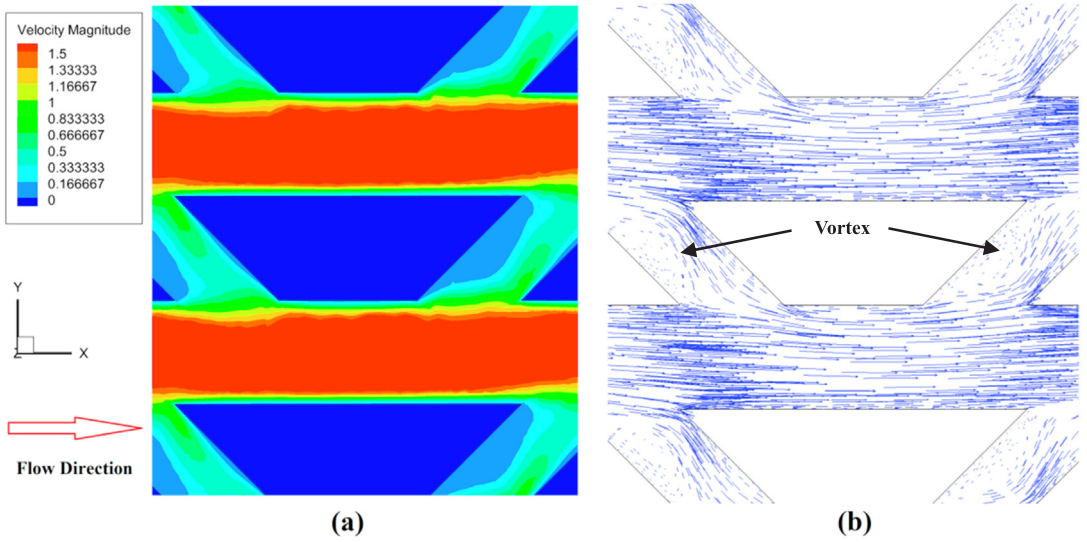

Fig. 10. (a) The flow velocity magnitude distribution (in m/s, *Re* = 295) and (b) velocity vectors around oblique fins on x-y plane (z = 0.25 mm, *Re* = 295) of 3# heat sink.

layer is limited by the shorter oblique fin compared to the long continuous traditional microchannel. Thus, as can be seen from the velocity vectors in Fig. 10(b), the velocity profile is rapidly renewed in every oblique fin. The combined effects of thermal boundary layer redevelopment and flow mixing can improve the heat transfer performance significantly, including reducing the maximum temperature of heat sink and maintaining better surface temperature uniformity. Meanwhile, as Steinke and Kandlikar [34] have pointed out, the

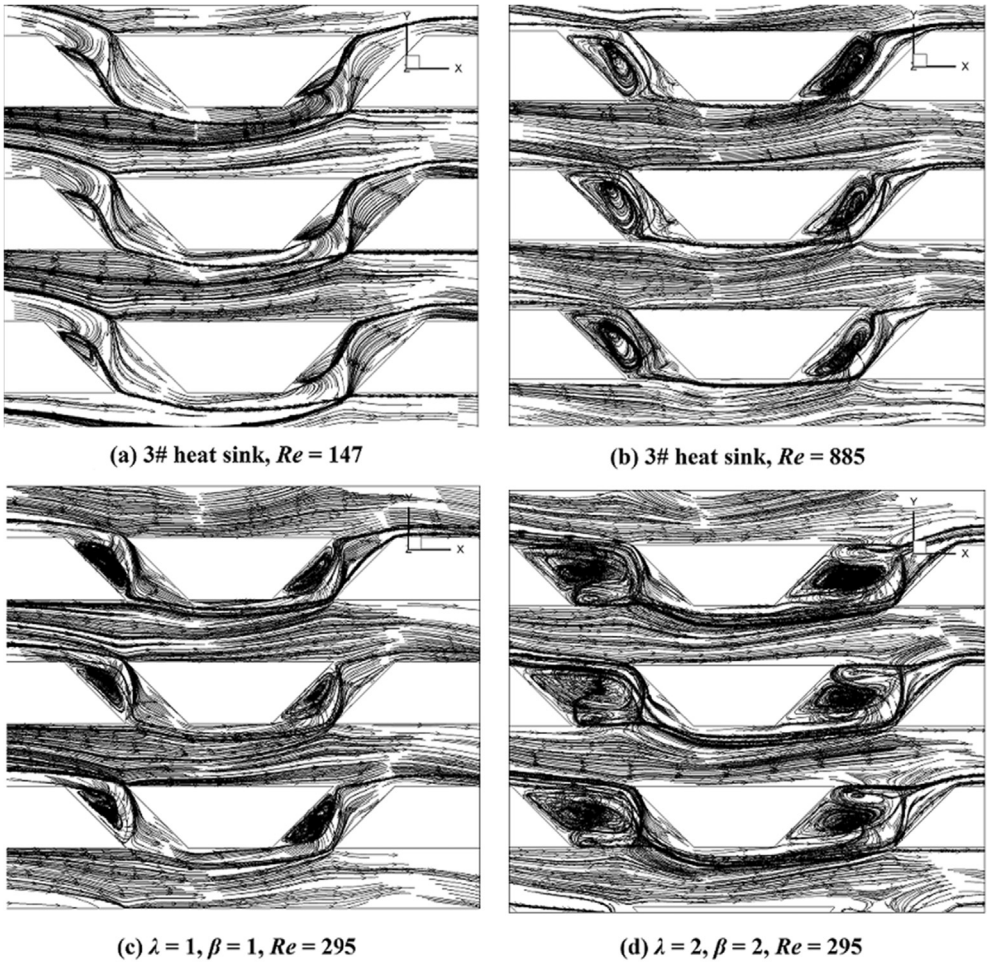

Fig. 11. Flow streamlines distribution around secondary fins. (a) 3# heat sink with *Re* = 147, (b) 3# heat sink with *Re* = 885, (c) 3# heat sink with *Re* = 295 and (d) heat sink (λ = 2, β = 2) with *Re* = 295.

pressure drop penalties could be a limiting factor for secondary flow devices. The fluid vortices will cause additional pressure loss because it needs extra kinetic energy to sustain its existence. Interestingly, a larger flow area can also reduce pressure drop [37]. Fig. 6 illustrates that pressure drop reduction can be obtained for most of the designed hybrid heat sink at $Re = 295$, which is caused by the increase of flow area provided by the secondary channels. However, the pressure drop ratio ($\Delta P/\Delta P_0$) becomes larger when Re increases, which indicates a worse flow performance. The foregoing analyses reveal an interesting fact that as to pressure drop, the secondary oblique channel has dual characteristics. On the one hand, if the Reynolds number is small enough, the effect of pressure drop reduction severs as the dominant role in the proposed heat sink design. Therefore, lower pressure drop compared with MMC heat sink can be obtained for most heat sink structures. However, with the increase of Reynolds number, it will lead more pressure loss compared with MMC heat sink due to the fluid vortices and flow friction, as shown in Fig. 9(f).

In order to further understand the effects of geometrical parameters and Reynolds numbers on the overall performance of MMC-SOC heat sink, Fig. 11 gives the flow streamlines distribution for different heat sinks and Reynolds numbers. A streamline is a curve that is instantaneously tangent to the velocity vectors within the flow field, and therefore a better flow visualization can be presented. For heat sink with different Reynolds number, as shown in Fig. 11(a) and (b), it is obvious that more flow streamlines will move into secondary channels for $Re = 885$ compared with those for $Re = 147$. In addition, the velocity field shows a very weak vortex generated within the secondary channel at $Re = 147$. At $Re = 885$, however, the vortex becomes much larger and stronger, which can be clearly seen from Fig. 11(b). Certainly, a better thermal performance and a worse hydraulic performance will be obtained in case of higher Reynolds numbers due to the fluid vortices and flow friction. Fig. 11(c) and (d) show the flow streamlines distribution for different heat sinks at the same Reynolds number. The secondary flow passage width d of heat sink ($\lambda = 2, \beta = 2$) is 300 μm, twice as large as that of the heat sink ($\lambda = 1, \beta = 1$). It can be observed that heat sink ($\lambda = 2, \beta = 2$) provides more flow area, which can draw more coolant flow through the secondary channel. The vortex of heat sink ($\lambda = 2, \beta = 2$) is also larger. However, the numerical results show that the heat sink ($\lambda = 1, \beta = 1$) has better overall performance than heat sink ($\lambda = 2, \beta = 2$). Thus, it is impossible to say anything definite about the thermal or hydraulic performance of different heat sinks at the same Reynolds number only through Fig. 11(c) and (d).

5. Conclusions

We propose a novel overall performance enhancement hybrid cooling scheme, employing both manifold arrangement and secondary flow in a microchannel heat sink. Fully 3D conjugate heat transfer analyses are performed to study the fluid flow and heat transfer characteristics of the hybrid heat sink. By changing relative secondary flow passage width λ and longer-edge length β, twenty-one types of heat sinks are designed. The following conclusions are drawn based on the numerical analyses:

1. Since it is unnecessary to consider the value of the convective heat transfer area, the existing evaluation method (the relationships between h, Nu, f, PEC and Re) is inapplicable for the comprehensive assessment of microchannel heat sink geometric optimization. Through the relationship between the total thermal resistance ratio (R_t/R_{t0}) and pressure drop ratio ($\Delta P/\Delta P_0$), we define a region named Design Optimization Area. By changing the velocity inlet boundary condition to pressure inlet boundary condition, we find that the heat sink with geometrical parameters of ($\lambda = 1, \beta = 1$) yields the best overall performance among those proposed heat sink designs.
2. Compared to traditional microchannel heat sink, the proposed hybrid design can greatly reduce the pressure loss through manifold arrangement because of the shorter flow length. Meanwhile, the secondary channels can enhance the heat transfer performance due to the combined effects of thermal boundary layer re-development and flow mixing. Compared to the original MMC heat sink, the proposed hybrid heat sink has a DOA, where the pumping power and the thermal resistance can be both reduced due to the introduction of the secondary channels. The numerical results show that the best hybrid heat sink can reduce the pressure drop by 1.91%, and simultaneously decrease the total thermal resistance by 19.15% compared to the original MMC heat sink at $Re = 295$.
3. For the proposed hybrid heat sink, the effects of the relative secondary flow passage width λ and longer-edge length β on the thermal and hydraulic performance are studied numerically. The results show that the heat sink will perform better when the values of λ and β both equal 1. In addition, the secondary oblique channel has a dual character. On the one hand, it can reduce the pressure loss at small Reynolds numbers for most heat sinks. However, it can also increase the pressure loss for most heat sinks at high Reynolds numbers.
4. As Re increases, the thermal resistance ratio (R_t/R_{t0}) becomes smaller and the pressure drop ratio ($\Delta P/\Delta P_0$) becomes larger, indicating a better thermal performance and a worse hydraulic performance. The effects of secondary channels on the pressure drop are dependent on both the geometrical parameters and Reynolds numbers. In addition, the number of heat sinks in DOA decreases with increasing Re, indicating fewer heat sinks can enhance the thermal and hydraulic performance simultaneously. The secondary flow field, including the flow velocity magnitude distribution, velocity vectors and flow streamlines, visually shows the hydraulic and thermal performance enhancements due to thermal boundary layer re-development and flow mixing.

Acknowledgement

This project was supported by the National Nature Science Foundation of China (Nos. 51825601, 51676108) and Science Fund for Creative Research Group (No. 51621062).

References

[1] K.K. Chu, T. Yurovchak, P.C. Chao, C.T. Creamer, Thermal modeling of high power GaN-on-diamond HEMTs fabricated by low-temperature device transfer process, Tech. Dig. – IEEE Compd. Semicond. Integr. Circuit Symp. CSIC. (2013) 6–9, https://doi.org/10.1109/CSICS.2013.6659246.
[2] Z.Y. Guo, Energy-mass duality of heat and its applications, ES Energy Environ. 1 (2018) 4–15, https://doi.org/10.30919/esee8c146.
[3] J. Li, G.P. Peterson, 3-Dimensional numerical optimization of silicon-based high performance parallel microchannel heat sink with liquid flow, Int. J. Heat Mass Transf. 50 (2007) 2895–2904, https://doi.org/10.1016/j.ijheatmasstransfer.2007.01.019.
[4] S. Liu, M. Chen, P.R. Chian, Thermal Analysis of High Power LED Array Packaging with Microchannel Cooler, Proc. of 7th International Conference on Electronics Packaging Technology, 2006, pp. 6–10.
[5] X.H. Yang, S.C. Tan, Y.J. Ding, J. Liu, Flow and thermal modeling and optimization of micro/mini-channel heat sink, Appl. Therm. Eng. 117 (2017) 289–296, https://doi.org/10.1016/j.applthermaleng.2016.12.089.
[6] X.L. Xie, Z.J. Liu, Y.L. He, W.Q. Tao, Numerical study of laminar heat transfer and pressure drop characteristics in a water-cooled minichannel heat sink, Appl. Therm. Eng. 29 (2009) 64–74, https://doi.org/10.1016/j.applthermaleng.2008.02.002.
[7] H.Y. Zhang, D. Pinjala, T. Poi-Siong, Thermal management of high power dissipation electronic packages: from air cooling to liquid cooling, Electron. Packag. Technol. 2003 5th Conf. (EPTC 2003). 2003, pp. 620–625, , https://doi.org/10.1109/EPTC.2003.1271593.
[8] W. Qu, I. Mudawar, Experimental and numerical study of pressure drop and heat transfer in a single-phase micro-channel heat sink, Int. J. Heat Mass Transf. 45 (2002) 2549–2565, https://doi.org/10.1016/S0017-9310(01)00337-4.
[9] S.G. Kandlikar, D. Schmitt, A.L. Carrano, J.B. Taylor, Characterization of surface roughness effects on pressure drop in single-phase flow in minichannels, Phys. Fluids. 17 (2005), https://doi.org/10.1063/1.1896985.
[10] Y. Zhu, D.S. Antao, K.-H. Chu, S. Chen, T.J. Hendricks, T. Zhang, E.N. Wang, Surface structure enhanced microchannel flow boiling, J. Heat Transf. 138 (2016) 091501, https://doi.org/10.1115/1.4033497.
[11] M. Yang, B.Y. Cao, W. Wang, H.M. Yun, B.M. Chen, Experimental study on capillary

filling in nanochannels, Chem. Phys. Lett. 662 (2016) 137–140, https://doi.org/10.1016/j.cplett.2016.09.016.
[12] B.Y. Cao, M. Yang, G.J. Hu, Capillary filling dynamics of polymer melts in nanopores: experiments and rheological modelling, RSC. Adv. 6 (9) (2016) 7553–7559, https://doi.org/10.1039/C5RA24991K.
[13] Y.X. Li, M.A. Alibakhshi, Y.H. Zhao, C.H. Duan, Exploring ultimate water capillary evaporation in nanoscale conduits, Nano. Lett. 17 (8) (2017) 4813–4819, https://doi.org/10.1021/acs.nanolett.7b01620.
[14] D.B. Tuckerman, R.F.W. Pease, High-performance heat sinking for VLSI, IEEE Electr. Dev. Lett. EDL-2 (1981) 126–129, https://doi.org/10.1109/EDL.1981.25367.
[15] S.G. Kandlikar, History, advances, and challenges in liquid flow and flow boiling heat transfer in microchannels: a critical review, J. Heat Transf. 134 (2012) 034001, https://doi.org/10.1115/1.4005126.
[16] R. Chein, J. Chen, Numerical study of the inlet/outlet arrangement effect on microchannel heat sink performance, Int. J. Therm. Sci. 48 (2009) 1627–1638, https://doi.org/10.1016/j.ijthermalsci.2008.12.019.
[17] R. Manikanda Kumaran, G. Kumaraguruparan, T. Sornakumar, Experimental and numerical studies of header design and inlet/outlet configurations on flow maldistribution in parallel micro-channels, Appl. Therm. Eng. 58 (2013) 205–216, https://doi.org/10.1016/j.applthermaleng.2013.04.026.
[18] Y. Sui, C.J. Teo, P.S. Lee, Y.T. Chew, C. Shu, Fluid flow and heat transfer in wavy microchannels, Int. J. Heat Mass Transf. 53 (2010) 2760–2772, https://doi.org/10.1016/j.ijheatmasstransfer.2010.02.022.
[19] H.A. Mohammed, P. Gunnasegaran, N.H. Shuaib, Numerical simulation of heat transfer enhancement in wavy microchannel heat sink, Int. Commun. Heat Mass Transf. 38 (2011) 63–68, https://doi.org/10.1016/j.icheatmasstransfer.2010.09.012.
[20] Y.T. Yang, H. Sen Peng, Numerical study of pin-fin heat sink with un-uniform fin height design, Int. J. Heat Mass Transf. 51 (2008) 4788–4796, https://doi.org/10.1016/j.ijheatmasstransfer.2008.02.017.
[21] S. Ndao, Y. Peles, M.K. Jensen, Multi-objective thermal design optimization and comparative analysis of electronics cooling technologies, Int. J. Heat Mass Transf. 52 (2009) 4317–4326, https://doi.org/10.1016/j.ijheatmasstransfer.2009.03.069.
[22] J. Yang, L. Li, L. Yang, J. Li, Uniform design for the parameters optimization of pin-fins channel heat sink, Appl. Therm. Eng. 120 (2017) 289–297, https://doi.org/10.1016/j.applthermaleng.2017.03.122.
[23] D. Yang, Z. Jin, Y. Wang, G. Ding, G. Wang, Heat removal capacity of laminar coolant flow in a micro channel heat sink with different pin fins, Int. J. Heat Mass Transf. 113 (2017) 366–372, https://doi.org/10.1016/j.ijheatmasstransfer.2017.05.106.
[24] F. Zhou, W. Zhou, Q. Qiu, W. Yu, X. Chu, Investigation of fluid flow and heat transfer characteristics of parallel flow double-layer microchannel heat exchanger, Appl. Therm. Eng. 137 (2018) 616–631, https://doi.org/10.1016/j.applthermaleng.2018.03.069.
[25] C. Leng, X.D. Wang, T.H. Wang, W.M. Yan, Multi-parameter optimization of flow and heat transfer for a novel double-layered microchannel heat sink, Int. J. Heat Mass Transf. 84 (2015) 359–369, https://doi.org/10.1016/j.ijheatmasstransfer.2015.01.040.
[26] G.M.H. and J.E. Eninger, Micro-channel heat exchanger optimization, Semicond. Therm. Meas. Manag. Symp. 1991. SEMI-THERM VII. Proceedings., Seventh Annu. IEEE. IEEE. (1991) pp. 59–63.
[27] D. Copelandl, M. Behniaz, W. Nakayamal, Manifold Microchannel eat Sinks: Ikothermial Analysis, IEEE Transac. Comp., Packag., Manuf. Technol.: Part A (1997).
[28] J.H. Ryu, D.H. Choi, S.J. Kim, Three-dimensional numerical optimization of a manifold microchannel heat sink, Int. J. Heat Mass Transf. 46 (2003) 1553–1562, https://doi.org/10.1016/S0017-9310(02)00443-X.
[29] E. Kermani, S. Dessiatoun, A. Shooshtari, M.M. Ohadi, Experimental investigation of heat transfer performance of a manifold microchannel heat sink for cooling of concentrated solar cells, Electron. Components Technol. Conf. 2009. ECTC 2009. 59th. (2009) pp. 453–459.
[30] S. Sarangi, K.K. Bodla, S.V. Garimella, J.Y. Murthy, Manifold microchannel heat sink design using optimization under uncertainty, Int. J. Heat Mass Transf. 69 (2014) 92–105, https://doi.org/10.1016/j.ijheatmasstransfer.2013.09.067.
[31] M.A. Arie, A.H. Shooshtari, S.V. Dessiatoun, E. Al-Hajri, M.M. Ohadi, Numerical modeling and thermal optimization of a single-phase flow manifold-microchannel plate heat exchanger, Int. J. Heat Mass Transf. 81 (2015) 478–489, https://doi.org/10.1016/j.ijheatmasstransfer.2014.10.022.
[32] S.N. Li, H.N. Zhang, X. Bin Li, Q. Li, F.C. Li, S. Qian, S.W. Joo, Numerical study on the heat transfer performance of non-Newtonian fluid flow in a manifold microchannel heat sink, Appl. Therm. Eng. 115 (2017) 1213–1225, https://doi.org/10.1016/j.applthermaleng.2016.10.047.
[33] K.P. Drummond, D. Back, M.D. Sinanis, D.B. Janes, D. Peroulis, J.A. Weibel, S.V. Garimella, A hierarchical manifold microchannel heat sink array for high-heat-flux two-phase cooling of electronics, Int. J. Heat Mass Transf. 117 (2018) 319–330, https://doi.org/10.1016/j.ijheatmasstransfer.2017.10.015.
[34] M.E. Steinke, S.G. Kandlikar, Single-phase heat transfer enhancement techniques in microchannel and minichannel flows, ASME, Conf. Microchann. Minichann. (2004) 141–148, https://doi.org/10.1115/ICMM2004-2328.
[35] Y.J. Lee, P.S. Lee, S.K. Chou, Enhanced microchannel heat sinks using oblique fins, ASME 2009 InterPack Conf. 2009, pp. 253–260, , https://doi.org/10.1115/InterPACK2009-89059.
[36] N. Raja Kuppusamy, R. Saidur, N.N.N. Ghazali, H.A. Mohammed, Numerical study of thermal enhancement in micro channel heat sink with secondary flow, Int. J. Heat Mass Transf. 78 (2014) 216–223, https://doi.org/10.1016/j.ijheatmasstransfer.2014.06.072.
[37] I.A. Ghani, N.A.C. Sidik, R. Mamat, G. Najafi, T.L. Ken, Y. Asako, W.M.A.A. Japar, Heat transfer enhancement in microchannel heat sink using hybrid technique of ribs and secondary channels, Int. J. Heat Mass Transf. 114 (2017) 640–655, https://doi.org/10.1016/j.ijheatmasstransfer.2017.06.103.
[38] G. Xie, H. Shen, C.C. Wang, Parametric study on thermal performance of microchannel heat sinks with internal vertical Y-shaped bifurcations, Int. J. Heat Mass Transf. 90 (2015) 948–958, https://doi.org/10.1016/j.ijheatmasstransfer.2015.07.034.
[39] L. Chai, G.D. Xia, H.S. Wang, Parametric study on thermal and hydraulic characteristics of laminar flow in microchannel heat sink with fan-shaped ribs on sidewalls - Part 2: Pressure drop, Int. J. Heat Mass Transf. 97 (2016) 1081–1090, https://doi.org/10.1016/j.ijheatmasstransfer.2016.02.076.